Analysis of Dynamic Crack Propagation in Elastomers by Simultaneous Tensile- and Pure-Shear-Mode Testing

Radek Stoček[1,2,3], Gert Heinrich[3,4], Michael Gehde[5], and Reinhard Kipscholl[6]

[1] PRL Polymer Research Lab., s.r.o., Nad Ovčírnou 3685, 760 01 Zlín, Czech Republic
[2] Centre of Polymer Systems, University Institute, Tomas Bata University in Zlin, Nad Ovcirnou 3685, 760 01 Zlin, Czech Republic
[3] Leibniz-Institut für Polymerforschung Dresden e. V., Hohe Straße 6, 01069 Dresden, Germany
[4] Technische Universität Dresden, Institut für Werkstoffwissenschaft, 01062 Dresden, Germany
[5] Technische Universität Chemnitz, Institut für Fördertechnik und Kunststoffe, 09107 Chemnitz, Germany
[6] Coesfeld GmbH & Co. KG, Tronjestr.8, 44319 Dortmund, Germany

Abstract. The present work proposes a new fracture mechanical testing concept for determination of dynamic crack propagation of rubber materials. This concept implements a method of simultaneous tensile- and pure-shear-mode testing. The present approach is based on an upgrade of the Tear Analyzer (Co. Coesfeld GmbH & Co. KG), on the fracture mechanics theory of dynamically loaded test specimens and on the definition of pure-shear states according to the test specimen's geometry ratio.

The main focus of this work can be divided into three parts. Firstly, it introduces the development of a method for analysis of dynamic crack propagation in filled rubber by simultaneous tensile- and pure shear mode testing. The servo-hydraulic machine with controlled temperature testing chamber is equipped with simultaneously operating two-mode test equipment that represents a new fracture testing method. This two-mode test allows the measurement of crack propagation on different rubber specimens simultaneously and under identical load. The data analysis allows a comparison between the two parallel running testing modes.

Secondly, this work deals with the development of a method for the defined creation of a notch in a rubber specimen. This method serves as a basis for the reproducible and reliable determination of fracture mechanical parameters for elastomers. After insertion of notches in a defined way, fracture tests under different loading conditions were performed. A significant influence on the notch geometry was observed in the test results. The results illustrated the importance of a defined and reproducible notching of elastomeric specimens.

Next, the analysis of crack propagation under dynamic loading conditions is practiced with this method. It is shown how the tearing energy and the crack

W. Grellmann et al. (Eds.): *Fracture Mechanics & Statistical Mech.*, LNACM 70, pp. 269–301.
DOI: 10.1007/978-3-642-37910-9_7

growth rate depend on the test specimen's geometry ratio and crack length. It is also demonstrated that the values for tearing energies and crack growth rates for short crack lengths in SENT, as well as in pure-shear test specimens, are identical. Another important aspect of the results is related to the different values of tearing energies and crack growth rates for cracks with short and large lengths in pure-shear test specimens. The results show the dependence of fracture behavior on the manufacture of the test specimens.

The new fracture mechanical testing concept offers a comparison between fracture behaviors of rubber materials independent of the test specimen's geometry.

Keywords: Rubber materials; Crack propagation; Tear Analyzer; Tearing energy; SENT; Pure-shear.

1 Introduction

The dynamic fracture behavior of elastomers has been intensively studied and published in a number of publications e.g. [1], [3], [3], [4], [5]. The mentioned works mainly deal with fracture mechanics of elastomers using different methods and testing equipment. Both methods allow an on-line evaluation of crack propagation, however, only one method is industrially used for the characterization of dynamic fracture behavior of elastomers: the tensile method. In the pure-shear method, the crack's propagation is caused due to uni-axial stress conditions in the crack tip.

The crack initiation and propagation mechanism of elastomeric materials is highly complex and always remains a subject of advanced research. An important criterion for characterization of dynamically loaded rubber materials is their resistance to fatigue crack growth. The problem of crack growth in rubber materials was first studied by Rivlin & Thomas [1]. In the publications of Lake & Lindley [2, 3], the authors first demonstrated fatigue crack growth dependent on the tearing energy of vulcanized rubber in the range of small as well as of critical strain. This dynamic crack growth behavior of vulcanized rubber was investigated in the SENT (Single Edge Notched Test) as well as in pure-shear test specimens, but the comparison of solutions for two different test specimen's geometry from the analysis is less well established.

The SENT test specimen is used in commercial studies of elasticity and fracture mechanics of rubber. However, in classical studies of fracture mechanics of rubber, the pure-shear test specimen featured prominently because of the amenability to a simple fracture mechanics analysis. The SENT test specimen consists of a thin, rectangular strip of rubber held by rigid clamps along its short edges and the definition is given by the geometry ratio L_0 (length or distance between the clamps in the un-deformed state)*:* Q (width of test specimen) ≥ 1. Compared to a SENT test specimen, the pure-shear test specimen consists of a thin, rectangular strip of rubber, but held by rigid clamps along its long edges. The

pure-shear test specimen is then defined by the geometry ratio $L_0 : Q << 1$. A simple FE-analysis of deformation of SENT as well as pure-shear test specimens represented by strain in the x-direction unambiguously showed the width of non-deformed range in the pure-shear compared to the SENT test specimen (s. Figure 1). However, when these test specimens are used to characterise the crack propagation of rubber, it is important to describe the influence of different test specimen areas as edge effect range (s. range *A* in the Figure 1-left) and pure-shear range (s. range *C*/2 in the Figure 1-right) on the crack length. Unfortunately, there is only limited information available in the literature (e.g. Yeoh [5]) on the influence of edge effects on the short crack length in the pure-shear test specimen, and limited information on the long crack in SENT test specimen.

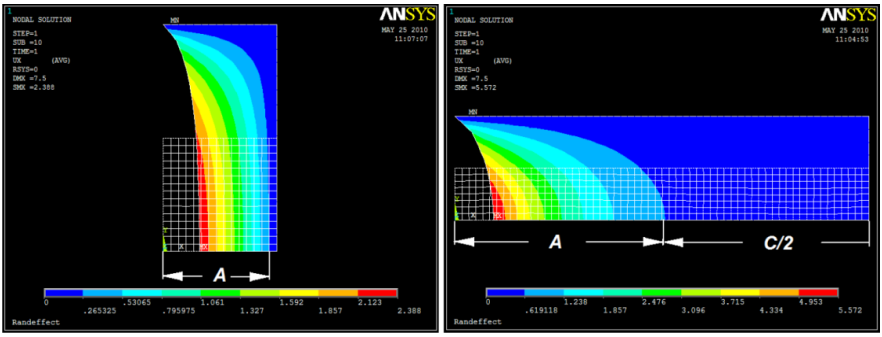

Fig. 1 FE - analysis of the deformation of quarter of SENT (left) as well as pure-shear (right) test specimens in the x-direction subjected to 100% tension

Considering the importance of the pure-shear and of the commonly used SENT test specimens, it is reasonable to consider the comparison of the crack propagation according to the different test specimen's geometry. Exact solution by traditional analysis of SENT and pure-shear test specimens is not possible, because of the use of different test machines and influence of test conditions. The new fracture mechanical testing concept based on a method of simultaneous SENT and pure-shear-mode testing was developed for use in the present work to describe the comparison of fracture behavior in SENT and pure-shear rubber test specimens.

Definition of the Test Specimen for Characterization of Fracture Behavior of Elastomers

The characterization of fracture behavior of elastomeric material is based on the analysis of notched test specimens. There is no information in the literature that deals with the definition of notch, or the exact definition of a test specimen's geometry. In the next paragraphs the test specimen's geometry and notch geometry will generally be defined for the characterization of fracture behavior in tensile as well as pure-shear methods.

The Figure 2 shows a schematic diagram of a test specimen's geometry as well as the geometry of a notch. The width of the test specimen is denoted as Q, the length is L_0 and the denotation of the thickness is B. The specification of the notch length is a_0, the actual crack's length a, and the radius of the notch tip is r_k.

The notch is defined as cut in the test specimen. The both of the opposed surfaces are defined as notch surfaces. The notch starts at the notch front edge and finishes at the notch tip.

The general definition of the notch's surface is:

$$\sin\alpha\cdot\cos\beta\cdot x-\cos\alpha\cdot\cos\beta\cdot y-\sin\beta\cdot z=0\,, \tag{1}$$

where the boundary conditions are:

$$z\in\left\langle-\frac{B}{2},\frac{B}{2}\right\rangle,\ y\in\left\langle-\frac{L_0}{2},\frac{L_0}{2}\right\rangle.$$

The notch's tip line is created from the intersection of the notch's surface and tip's plane of notch. The tip's plane of notch is defined with a normal vector, which is oriented in the notch's surface and has an orthogonally orientation to the tip line of the notch. The equation of the tip's plane of notch is defined as follows:

$$\begin{aligned}&\left[\sin\alpha\cdot\sin\beta\cdot\sin\gamma-\cos\alpha\cdot(1-\cos\gamma)\right]\cdot x+\\&+\left[-\cos\alpha\cdot\sin\beta\cdot\sin\gamma-\sin\alpha\cdot(1-\cos\gamma)\right]\cdot y+\\&+(\cos\beta\cdot\sin\gamma)\cdot z+a_0\cdot(1-\cos\gamma)-\sin\gamma=0\,.\end{aligned} \tag{2}$$

The front plane belongs to the yz-plane and is expressed with following general equation:

$$x=0\,. \tag{3}$$

The back plane is oriented parallel to the yz-plane. The next equation defines the back plane:

$$x-Q=0\,. \tag{4}$$

The side planes are located parallel to the xy-plane, and they are described as follows:

$$z-\frac{B}{2}=0\,;\ z+\frac{B}{2}=0\,. \tag{5}$$

The first parallel plane to the xz-plane is denoted as the upper plane:

$$y-\frac{L_0}{2}=0 \tag{6}$$

and the second one with the definition:

$$y + \frac{L_0}{2} = 0 \tag{7}$$

is denoted as the bottom plane.

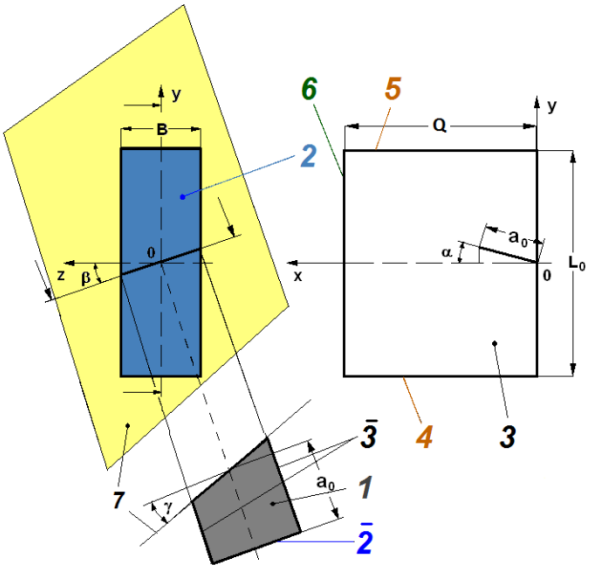

Fig. 2 Schematic diagram of the test specimen with: 1 – notch's surface, $\bar{2}$ – front edge of the notch, 2 – front plane, $\bar{3}$ – side edges of the notch, 3 – side plane 4 – bottom plane, 5 – upper plane, 6 – back plane, 7 – tip's plane of notch

Tearing Energy

An important quantity for fracture mechanical investigations is the tearing energy *T*, i.e. the energy released per unit area of crack surface growth. It was first introduced by Griffith [6] for metallic materials and Rivlin & Thomas [1] formulated the tearing energy for elastomers. It proposes that the strain energy release rate is the controlling parameter for crack growth and it is mathematically defined as,

$$T = -(\delta W/\delta A). \tag{8}$$

Where, *T* is tearing energy, *W* is the elastic strain energy, *A* is the interfacial area of crack and partial derivative denotes that no external work is done on the system.

In the language of geometry they defined the tearing energy for rubber material in SENT as well as in pure-shear test specimens. For SENT test specimens with a notch on one side, it is determined as follows:

$$T_t = 2 \cdot k \cdot w \cdot a\,, \tag{9}$$

Where w is the strain-energy-density stored in the un-notched test specimen; a - crack length; k = strain-dependent term. An approximate relation for k was determined by Lake [7]:

$$k = \frac{\alpha}{\sqrt{\lambda}} = \frac{\alpha}{\sqrt{1+\varepsilon}}\,, \tag{10}$$

where λ = extension ratio; ε = strain and α is a fit parameter. Furthermore, it was found by Klüppel [8] that the parameter α does not agree with the literature value $\alpha = \pi = 3.14$ proposed by Gent [9]. The value of the parameter α has been determined by Klüppel [8] for various samples between 1.2 and 3.1. In the presented work $\alpha = \pi = 3.14$ was used. Thus the equation (1) takes the form

$$T_t = \frac{2 \cdot \alpha}{\sqrt{\lambda}} \cdot w \cdot a = \frac{2 \cdot \alpha}{\sqrt{1+\varepsilon}} \cdot w \cdot a\,. \tag{11}$$

Figure 3 shows schematically the geometry of SENT test specimen, in which, according to FE-analysis of the un-notched geometry, the width of test specimen Q consists of a region of edge effect A. Thus the notch in the edge of the test specimen influences a width of a region D that includes a complicated strain around the crack tip.

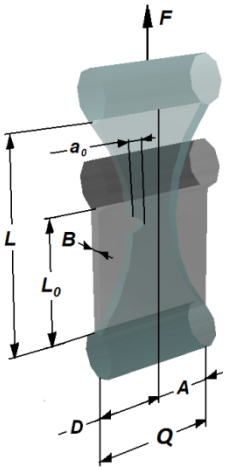

Fig. 3 Schematic diagram of SENT test specimen

The pure-shear test specimen first defined by Rivlin & Thomas [1] is schematically visualized in the Figure 4. Usually, the notch length a_0, which develops into the crack length a, is sufficiently long compared to the length of test specimen L_0. The test specimen can be divided into different regions. Region A_1 is unstrained and region C-D is in pure-shear state, whereas the region C is identical

to the pure-shear state region *C* in the un-notched test specimen visualized in the Figure 1 (right) and is geometrically defined as follows:

$$\lambda(x) = \frac{dx}{dx_0} = 1$$
$$\lambda(y) = \frac{dy}{dy_0} = \frac{y}{y_0} = \varepsilon(y) + 1 \quad \Rightarrow \quad \begin{bmatrix} x \\ y \end{bmatrix} = \begin{bmatrix} 1 & 0 \\ 0 & \varepsilon(y)+1 \end{bmatrix} \cdot \begin{bmatrix} x_0 \\ y_0 \end{bmatrix}. \quad (12)$$

Furthermore, there is an area of complicated strain around the crack tip in region *D*, and a region of edge effect shown as *A* that is identical with the edge effect region *A* of the un-notched test specimen visualized in Figure 1 (right). If the maximum cyclic deformation remains constant and the crack length is increased by *da*, the region of complicated strain *D* moves along by *da*, but the pattern of strain, and hence the energy stored, remains unaltered. As a result, the net effect causes a decrease of region *A* and an increase of region *C* by a volume $L_0 \cdot t \cdot da$ and, thus, a decrease of the total elastic energy $w \cdot L_0 \cdot t \cdot da$, where *w* is the strain-energy-density in the pure-shear region *C*.

For a pure-shear test specimen's geometry, the tearing energy T_p is considered by Rivlin & Thomas [1] to be independent of the crack length:

$$T_p = w \cdot L_0 \quad (13)$$

The strain-energy-density *w* can be determined from the measurement of the tensile stress-strain curve of the un-notched test specimen.

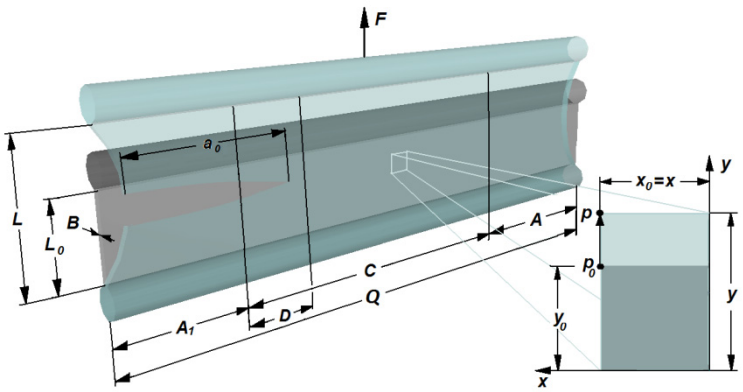

Fig. 4 Schematic diagram of a pure-shear test specimen with the visualisation of regions under different stress conditions

Fracture Mechanical Treatment of Failure

Gent, Lindley and Thomas [10] determined experimentally the crack growth rate *da/dn* in dependence on the tearing energy *T* for rubber materials.

Figure 5 shows the typical relationship for a rubber material on a double logarithmic plot. Lake & Lindley [3] divided this plot into 4 regions that characterize different tear behaviors. The crack growth rate *da/dn* depends on the tearing energy *T* in each of the 4 regions in a characteristic manner.

As long as the value of tearing energy *T* is lower than T_0, crack growth proceeds at a constant rate *r* and the crack growth is independent of the dynamical loading, but affected by the environmental attack.

$$T \le T_0 \Rightarrow \frac{da}{dn} = r \tag{14}$$

In region II between T_0 and T_1 one finds a transition between a nucleation and propagation of crack growth:

$$T_0 \le T \le T_1 \Rightarrow \frac{da}{dn} = A\left(T - T_0\right) + r \tag{15}$$

After this transient state the crack propagates in a region between T_1 and T_C of stable crack growth which is denoted as region III. The relationship between fatigue crack growth rate *da/dn* and tearing energy is described by Paris & Erdogan [11] with the power-law:

$$T_1 \le T < T_C \Rightarrow \frac{da}{dn} = b \cdot \Delta T^m, \tag{16}$$

where *b* and *m* are material constants.

In the last region, IV, the tearing energy T_C proceeds to the instable state of crack growth and the crack growth rate will become essentially infinite.

$$T \approx T_C \Rightarrow \frac{da}{dn} = \infty \tag{17}$$

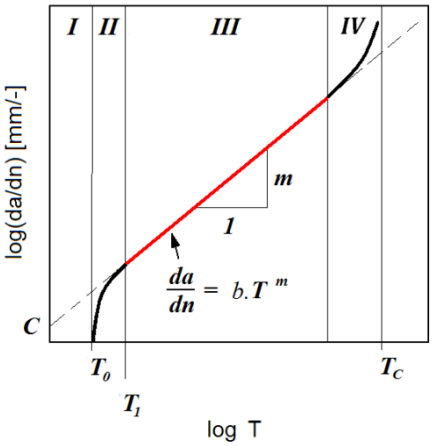

Fig. 5 Double logarithmic plot of crack growth rate *da/dn* vs. tearing energy *T* for rubber material [3]

Region III was utilised as the region that corresponds most closely to crack growth rates found in the engineering fatigue range. In this work, an experimental simultaneous analysis of SENT and pure-shear test specimens was performed according to this region to compare the stable crack growth in both of the test specimens depending on the notch and crack lengths.

2 Evaluation of Tearing Energy by Using Finite Element Analysis

The simplicity in shape of the pure-shear test specimen makes it suitable for an evaluation of the tearing energy in test specimens by using FEM, whereas the test specimen's geometry ratio $L_0 : Q$ was taken into account. The first evaluations of tearing energy were performed by Yeoh [5], where the geometry ratio $L_0 : Q$ = 1:5 was studied and the different tearing energy influenced by crack length was observed.

The tearing energy has been evaluated using non-linear finite element analysis with software ANSYS by using the 6-parameters Ogden material model. Test specimens with three different geometry ratios $L_0 : Q$ = 1:12; 1:4 and 1:1.5 with constant length L_0 and modified width Q were modeled to study the effect of different geometry ratios. Taking advantage of symmetry, only one quarter of each test specimen was modeled, meaning that two crack growths in opposite edges were simulated. The simulation was performed by 10, 30 and 50 % strain applied on the long edges of modeled test specimen.

Figure 6 shows FEM results for the dependence of tearing energy on crack length for a test specimen based on styrene-butadiene rubber (SBR) with geometry ratios $L_0 : Q$ = 1:12 and 1:4, whereas the width Q was constant and the length L_0 was varied. The simulation was subjected to 10, 30 and 50% strain. The notation, which is used in the diagrams, is explained in Figure 7.

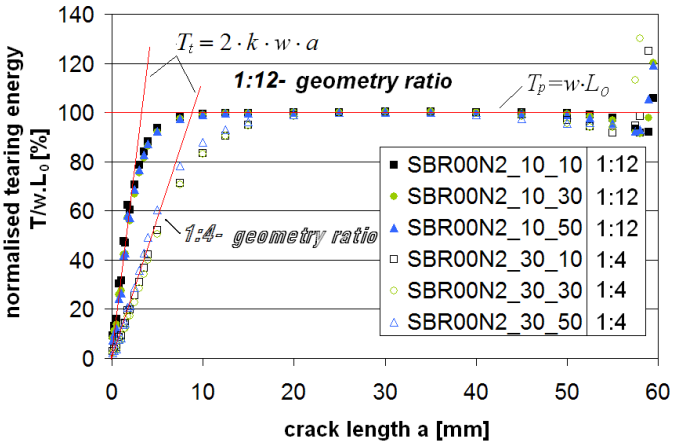

Fig. 6 Dependence of tearing energy on crack length for edge cracks in test specimens with geometry ratios 1:12 and 1:4 at various strains

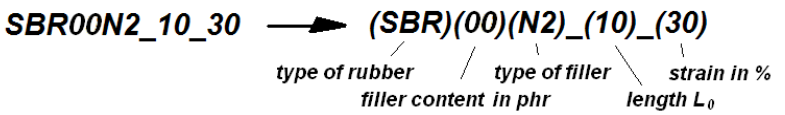

Fig. 7 Specification of the notation used in the diagrams

Figure 6 shows that independent of the geometry ratio, the tearing energy is approximately linearly dependent on a for short crack lengths according to the equation (1). This narrow range of the applicability of the Rivlin & Thomas theory changes into the non-defined transition of dependence of tearing energy on crack length. The calculation of tearing energy dependent on crack length shows in the center of the test specimen a region in which the tearing energy is independent of crack length. This region is deformed in the pure-shear state and formulated by the equation (5). The last region of the large crack lengths varied from the constant state of tearing energy by reason of the symmetric model of the test specimen. The comparison of the results obtained for the geometry ratios 1:12 and 1:4 shows a relatively small central region of the test specimen for the geometry ratio 1:4 deformed in the pure-shear state. On the other hand, it demonstrated the independence of various strains fromthe different geometry ratios.

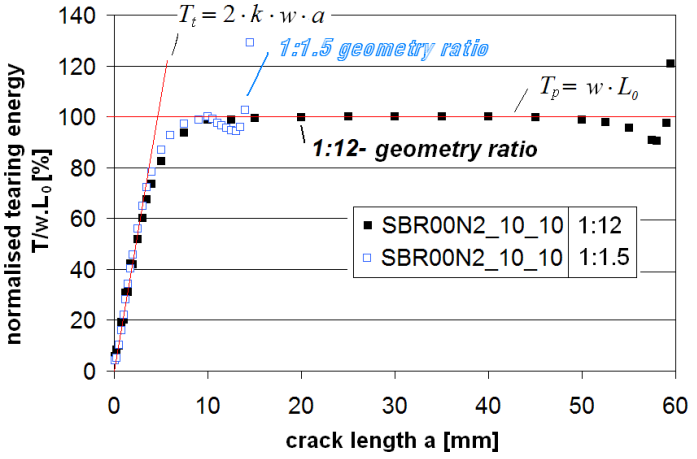

Fig. 8 Dependence of tearing energy on crack length for edge crack in test specimens with geometry ratios 1:12 and 1:1.5 at strain 10%

Figure 8 shows the FEM results of an edge crack in test specimens with geometry ratios 1:12 and 1:1.5 at strain 10%. The higher geometry ratio 1:1.5 was achieved by means of constant length L_0 and various widths Q. The geometry ratio 1:1.5 presents the geometry of the SENT test specimen. The simulation proved an identical slope of the linear dependence of tearing energy on crack length for small cracks a suggested by equation (1), in both test specimens with different geometry ratios. This documented that the identical crack growth in the region of availability of the equation (1) provided the same length L_0 of test specimens defined with different geometry ratios. There is no region of tearing energy independent of crack length in the center of the test specimen with the geometry ratio 1:1.5 according to the FEM simulation performed in the Figure 1 (left).

The FEM simulations were performed subjected to stable crack growth in rubber test specimens under dynamic loading. This basic fact according to the power-law described with equation (8) forms a real hypothesis for the constant crack growth velocity in the regions of availability of equations (1) and (5). Therefore, the insignificant dependence of the of equations (1) and (5) on the different rubber materials was established. The crack growth velocity could be an important indicator for the dependence of tearing energy on crack growth rate, which can be determined by experimental analysis.

3 Development of Testing Equipment for the Analysis of Dynamic Crack Propagation by Simultaneous Tensile and Pure-Shear Mode Testing

The new testing equipment for the analysis of dynamic crack propagation in filled rubber by simultaneous tensile and pure-shear mode testing is based on the redevelopment of the commercially and industrially used Tear Analyzer made by the company Coesfeld GmbH & Co. KG The Tear Analyzer available at the Technical University of Chemnitz was used for the development of this new testing method.

3.1 Design of Commercial Tear Analyzer

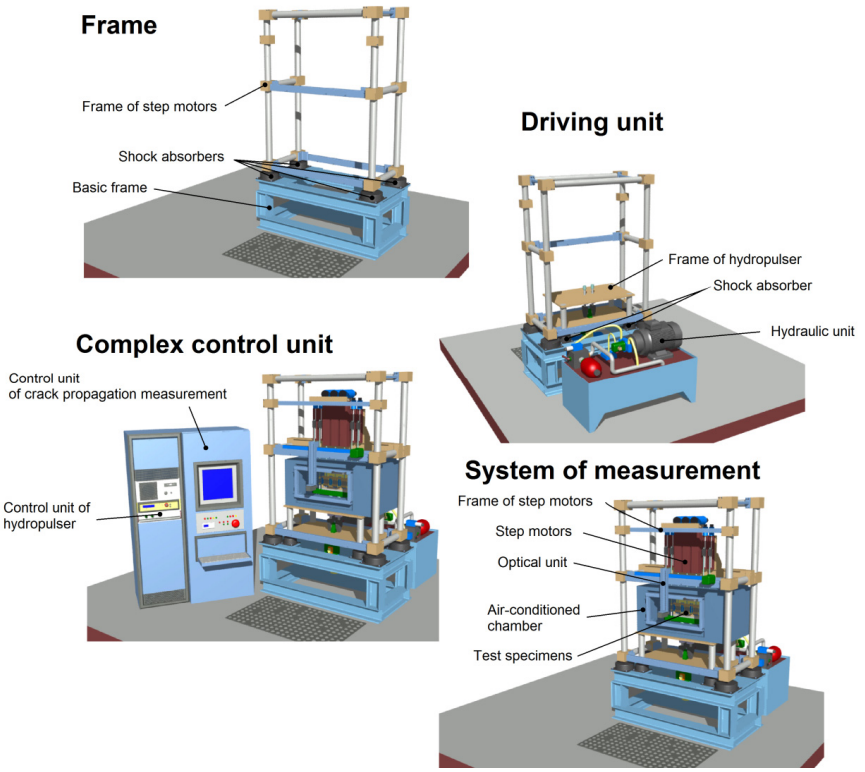

Fig. 9 Design of commercial Tear Analyzer

3.2 Basic Functionality of the Redeveloped Tear Analyzer

A schematic function diagram is shown in Figure 10 of the Tear Analyzer for investigating the fatigue crack growth of rubber materials by simultaneous tensile and pure-shear mode testing. It is possible to measure four tensile and three pure-shear test specimens simultaneously. Each bottom clamp attachment of the samples is fixed to the traverse. The traverse is connected to the piston, whereby it dynamically powers a hydropulzer. The hydropulzer is driven by a frequency sweep generator powered sinusoidal waveform, within the frequency range 0,1 - 50 Hz. The Amplitude of displacement is adjusted up to 20 mm in extension. Each upper clamp attachment of the samples is fixed to the load cell and its corresponding sample clamp attachment is connected to a separate computer-controlled stepping motor to ensure constant pre-stress during the whole time of analysis.

The crack growth of each rubber specimen is monitored through an image processing system with a CCD monochrome camera mounted on the linear motion axis system. The camera moves along the x-axis from specimen to specimen and takes a picture of the involved sample. The picture is then transferred to a frame grabber and stored. After the picture has been digitalized, the software localizes in situ the crack position and determines the contour length by following the black and white boundary line of the crack. The infinitesimal enlargement of crack surface area through dynamic loading can be determined according to Rivlin & Thomas criterion [1].

The separate connection of each stepping motor with control unit 2 additionally supplies the Tear Analyzer with a quasi-static testing method. This method is realized as follows: the hydropulzer is stopped and the stepping motor can move with the upper clamp attachments of the sample in the enabled range. The range of deformation is 300 mm. Each load cell transfers the stress-strain data to the computer and CCD camera system grabbed the crack propagations in the involved sample.

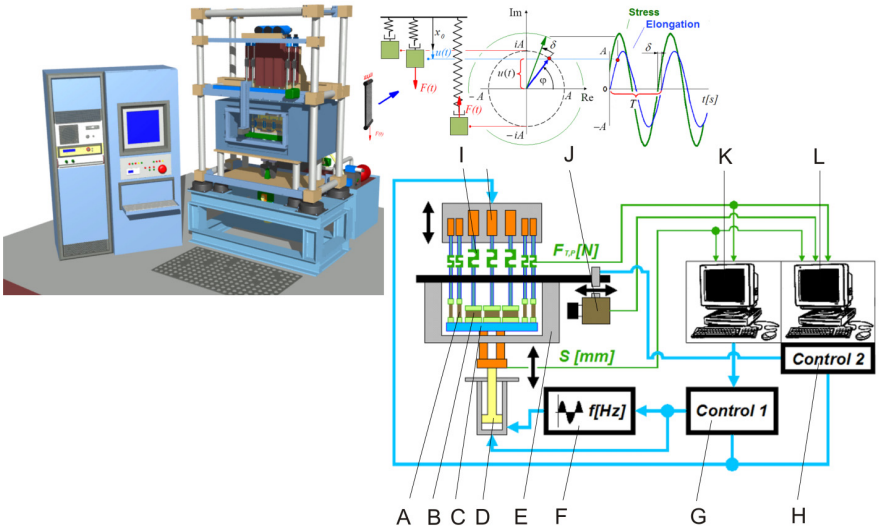

Fig. 10 Schematic and functional diagram of the test machine: A-tensile test piece; B-pure-shear test piece; C-traverse; D-hydropulzer; E-isolated chamber; F-frequency generator; G-control unit 1; H-control unit 2; I-load cells; J-CCD monochrome camera; K-PC1; L-PC2;

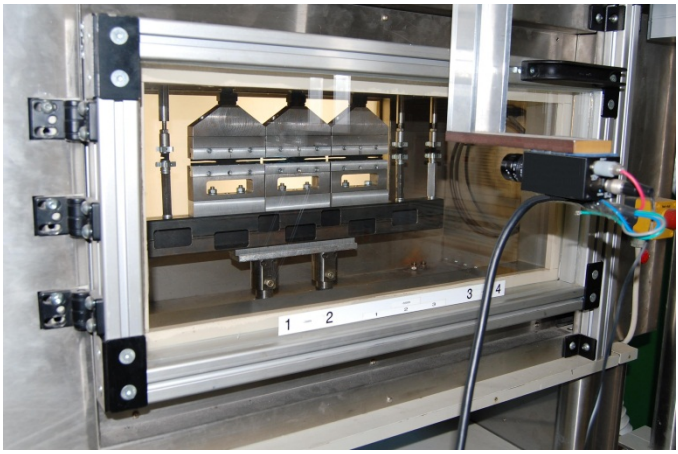

Fig. 11 The real visualization of the air-conditioned chamber with camera and SENT as well as pure-shear test specimens

3.3 Adjusting of the Tear Analyzer's Design for Measurement at Higher Loading Conditions

The Tear Analyzer is dynamically working mechanical equipment, which is characterized with natural mode shapes and frequencies dependent on the design body. Why is it important to measure the natural mode shapes and frequencies? At certain natural frequencies of the structure, a small amount of input force can cause a very large response. The redevelopment of Tear Analyzers caused measurement at higher forces and thus the design of the structure must be controlled for the response of the system in changed loading conditions. Certainly, two of the most important areas of structural dynamics testing is that of experimental and FEM modal analysis. The identification of dynamic properties of the Tear Analyzer has been performed using FEM modal analysis, because of the very complicated realization of experimental analysis. The FEM analysis simplifies the establishment of natural modal shapes because of the possibilities to modify the structure before any prototype is available for experimental measurement. The structure can be modified much cheaper, faster and easier than it could be redesigned for the real prototype. The building of the model with up to date hardware is the next advantage of the FEM method. The FEM model can predict a structure's behavior under real world dynamic operating conditions.

Discrete Model of the Tear Analyzer

For the creation of a discrete model of the Tear Analyzer, it is assumed that a solid material can be represented as a collection of particles corresponding to the material model interacting among themselves in different directions. The discrete model was created with respect to the weak points of the Tear Analyzer‘s structure. The most important weak point was expected in the interaction between

the rigid clamps and rubber test specimens, because of the high difference of their mechanical behavior.

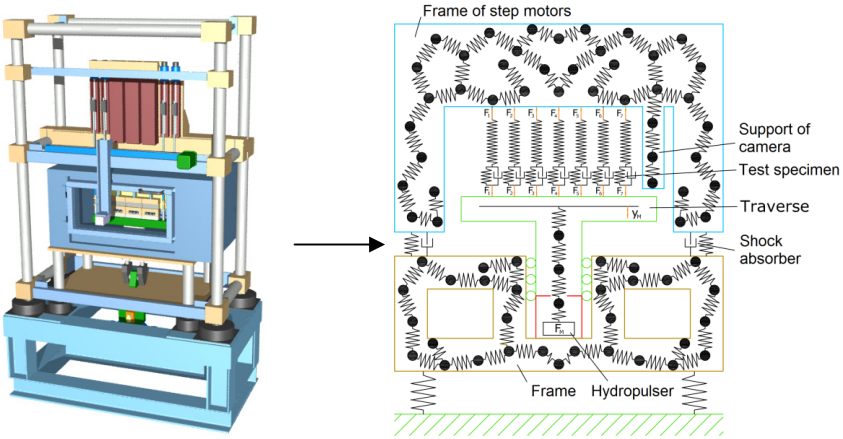

Fig. 12 Discrete model of the Tear Analyzer

Frequency Analysis and Optimizing of the Tear Analyzer's Discrete Model
The complex model of the Tear Analyzer has been calculated using the software ANSYS. The model of the structure consists of 62.981 elements, 118.152 nodes and 351.984 degrees of freedom. The calculation of natural mode shapes has been established in the range of frequency from 0.1 to 20 Hz.

$\omega_1 = 11$ Hz

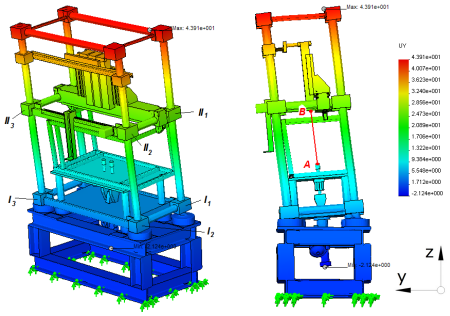

Fig. 13 The first modal mode shape

$\omega_2 = 14{,}5$ Hz

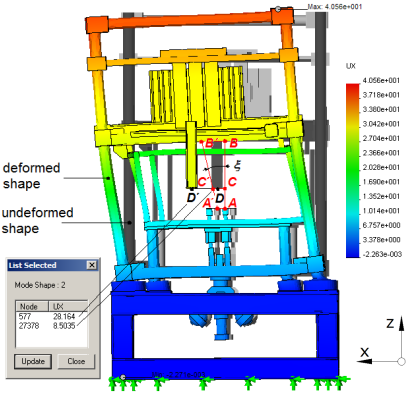

Fig. 14 The second modal mode shape

The calculation showed that the first two natural mode shapes are caused by the frequencies ω_1 = 11 Hz and ω_2 = 14.5 Hz. The first natural mode shape is caused by forwarding deformation, and the second one by longitudinal deformation.

The first natural mode shape has no influence on the distance between points A and B. Therefore, the measurement will be not influenced at the loading frequency 11 Hz. The second natural mode shape with deformation of the longitudinal direction significantly influences the distance between points A and B. The calculation of the distance showed a difference of about 0.0542% (s. Figure 14). The second natural mode shape caused the moving of the camera's holder (s. Figure 14, distance between C-C` and D-D´). The modal distance was established at the values $x_{rC\text{-}C'}$ = 8,5 and $x_{rD\text{-}D'}$ = 28,2. This result shows the importance of the attunement of the structure on natural mode shapes at frequencies higher than 20 Hz. As the natural mode shapes showed, this will be reached with stabilization or reinforcement of the frame. Figure 15 shows the first modal mode shape of the re-supported Tear Analyzer occurring outside of the frequency range of 0.1 to 20 Hz at ω_{1v} = 21,8 Hz.

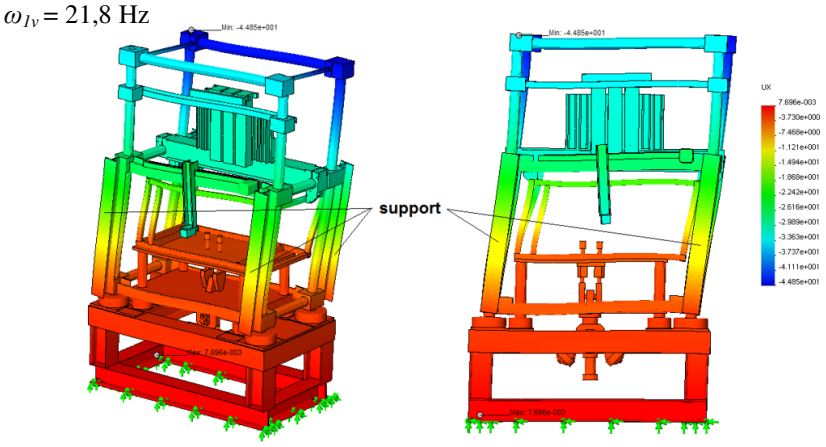

Fig. 15 The first modal mode shape of the re-supported Tear Analyzer

4 Experimental Section

4.1 Materials and Sample Preparation

For experimental investigations, unfilled and filled elastomers were compounded in an intermeshing mixer by DIK Hannover. Vulcanization of the samples was

Table 1 Composition of the materials investigated; data in phr

No	Label	NR	SBR	EPDM	CB N234	CB N234 Mas.bat.	Sulph.	ZnO	Stear. acid	ASM	T_{90} [min]
1	NR00	100	-	-	-	-	1	3	1	1,5	20,9
2	NR20N2	100	-	-	20	-	1	3	1	1,5	7,6
3	NR40N2	100	-	-	40	-	1	3	1	1,5	11,3
4	NR60N2	100	-	-	60	-	1	3	1	1,5	9,7
6	SBR00	-	100	-	-	-	1	3	1	1,5	5,1
7	SBR20N2	-	100	-	20	-	1	3	1	1,5	4,7
8	SBR40N2	-	100	-	40	-	1	3	1	1,5	3,7
9	SBR60N2	-	100	-	60	-	1	3	1	1,5	2,5
11	EPDM00	-	-	100	-	-	1	3	1	1,5	12,7
12	EPDM20N2	-	-	100	20	-	1	3	1	1,5	11,1
13	EPDM40N2	-	-	100	40	-	1	3	1	1,5	8,4
14	EPDM60N2	-	-	100	60	-	1	3	1	1,5	3,4
16	S-NR60N2	50	50		60	-	1	3	1	1,5	3,9
17	S-E60N2N	-	50	50	60	-	1	3	1	1,5	5,8
18	S-E60N2M	-	50	50	-	60	1	3	1	1,5	6,3

performed semi-efficiently with sulfur and accelerator (CBS-N-Cyelohexy1-2-benzothiazole sulfonamide and DPG-Dyphenylguanidine) in a heat press up to 90 % of the vulcameter torque maximum (T 90-time). As reinforcing filler, a constant amount (20, 40 and 60 phr) of carbon black type N234 was used. In the first phase the basic polymers were studied: natural rubber (NR), solution-styrene-butadien rubber (SBR) with 50% vol. vinyl and 25% vol. styrene and an amorphous ethylen-propylen-dien rubber (EPDM; Keltan 512). In the second phase, the blends consisting of combinations of NR, SBR or EPDM were investigated. All samples were compounded with the processing additives stearic acid and ZnO and protected against aging by IPPD. The ingredients are listed in Table 1. Standard SENT ($L_0 : Q$ = 1:1) and pure-shear ($L_0 : Q$ = 1:8) test specimens based on all types of compounds were cured and used for the fatigue experiments.

4.2 Influence of the Notch Procedure on Crack Propagation in Elastomers

The mechanisms of crack initiation and propagation in elastomeric materials are the subject of high scientific interest, because at present it is still not exactly known how these processes start and how they proceed under quasi-static as well as dynamic loading conditions. Therefore, the effect of the notch's geometry on crack propagation has been studied. A new method for the defined insertion of a notch into a rubber specimen was developed. This method serves as a basis for the

reproducible and reliable determination of fracture mechanical parameters for elastomers. After the insertion of notches in a defined way into the test specimens with the geometry ratio $L_0 : Q$ = 1:2, fracture tests under quasi-static loading conditions were performed.

The method of the notching is based on the blade razor insertion in the orthogonal direction to the supposed main strain of test specimen. The schematic diagram of the notching process and the created notch's surface are shown in the Figure 16. The principle of the defined insertion of the blade razor into the test specimen was realized with the redeveloped instrumented tensile test machine. Thus, the quantitative method of notching with exact positioning and length of the notch could be obtained.

For the investigation of the notch geometry and position influence on the crack propagation, four different notch's geometries have been realized using this new method. The Table 2 shows the realized notch geometries according to the definition of the test specimen and notch geometry (s. Figure 2). The geometry of the notch denoted 1 is created exactly orthogonally to the main stress. The second notch is defined with $\alpha = 0°$ and $\beta = \gamma = 20°$. The geometry of the notch denoted 3 has an orientation defined with $\alpha = \beta = \gamma = 10°$ and the last notch occurs with geometry $\alpha = 20°$, $\beta = \gamma = 0°$.

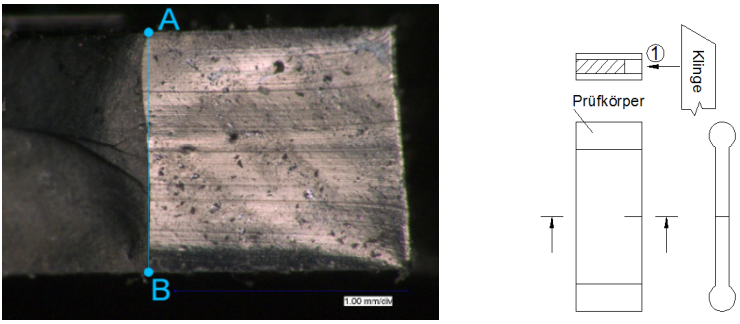

Fig. 16 Vizualization of the method of notching process and created notch's surface

Table 2 List of the notch geometries

	a_0 [mm]	α [°]	β [°]	γ [°]
1	2	0	0	0
2	2	0	20	20
3	2	10	10	10
4	2	20	0	0

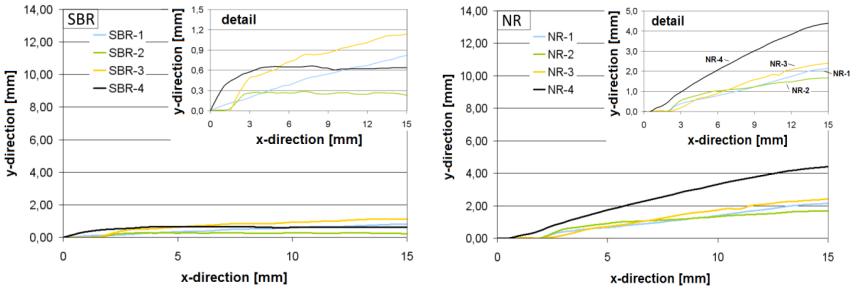

Fig. 17 The outline of the propagated crack in SBR (left) and NR (right), where: blue – notch's geometry 1 with $\alpha = \beta = \gamma = 0°$, green – notch's geometry 2 with $\alpha = 0°$, $\beta = \gamma = 20°$, orange – notch's geometry 3 with $\alpha = \beta = \gamma = 10°$ and black – notch's geometry 4 with $\alpha = 20°$, $\beta = \gamma = 0°$

Experimental data are plotted in Figure 17 and show the outlines of the propagated cracks in SBR (left) and NR (right) in the xy-direction. The influence of the notch geometry on the crack propagation is unambiguously evident. We found a higher deviation of crack growth outlines from the orthogonal direction to the main stress in the compound based on NR in comparison to the rubber based on SBR.

The slopes of the crack growth outlines measured in SBR demonstrate the parallel propagation of cracks in the case of a notch's geometry denoted 1: $\alpha = \beta = \gamma = 0°$. The other more complicated notches induce a substantial discrepancy when compared with the orthogonal direction to the main strain. The observed outlines of crack growth in rubber based on NR show an increase in the deviation from the orthogonal direction to the main strain over the whole effective test specimen's width. That effect occurs in strain-crystallizing rubber, such as analyzed natural rubber.

4.3 Investigations about Pure-Shear Width and Minimal Notch Length in Test Specimens

Because of the different strained regions in the pure-shear test specimen (s. Figure 4) it was necessary to investigate and to define the width of the pure-shear region and thus the minimum length of the notch for the initiation of crack propagation for the analysis of dynamic crack growth in the pure-shear region of a test specimen. The theory assumes that the pure-shear region is completely unstrained in the orthogonal direction to the main stress. The objective of the observation was to determine the width of this region. A schematic visualization of strained and unstrained regions in a stressed test specimen is shown in Figure 18. The region *C* visualizes the pure-shear region and the other regions denoted with *A* correspond with regions of deformed edges.

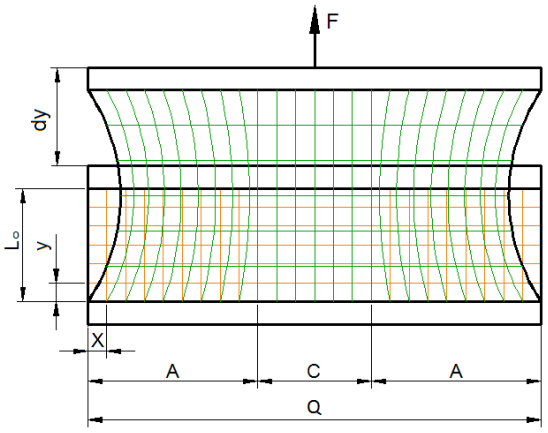

Fig. 18 Schematic visualization of determination of the width *C* of pure-shear area

Standard test specimens based on non-reinforced and reinforced SBR with amounts (20, 40 and 60 phr) of carbon black type N234, with different geometry ratios L_0:Q in the range of 1:12 to 1:4 and without initial cracks have been investigated first using FEM and second experimentally. The analyzed test specimen's geometries are listed in the Table 3.

Table 3 List of analyzed test specimen's geometries

No.	Length L_0 [mm]	Width Q [mm]	Geometry ratio L_0:Q
1.	10	120	1:12
2.	15	120	1:8
3.	20	120	1:6
4.	30	120	1:4

The width of the pure-shear region has been evaluated using non-linear finite element analysis with the software ANSYS by using the 6-parameter Ogden material model. Taking advantage of symmetry, only one quarter of each test specimen was modeled. The simulation was performed by different strains from 10 to 100 % of the test specimen's length L_0 applied on the long edges of the modeled test specimen.

The newly developed experimental method is based on tensile analysis of test specimens, wherein the surface of the test specimen is modified with a white squared layer. The stretched white squared layer is evaluated in an optical system that measures the displacement of the vertical layers in the points of intersection with the horizontal axis of the test specimens. The points with constant

displacement over the whole stretched layers define the pure-shear region. The applied strain corresponds with the FEM calculation and was set at different strains from 10 to 100 % of test specimen's length L_0.

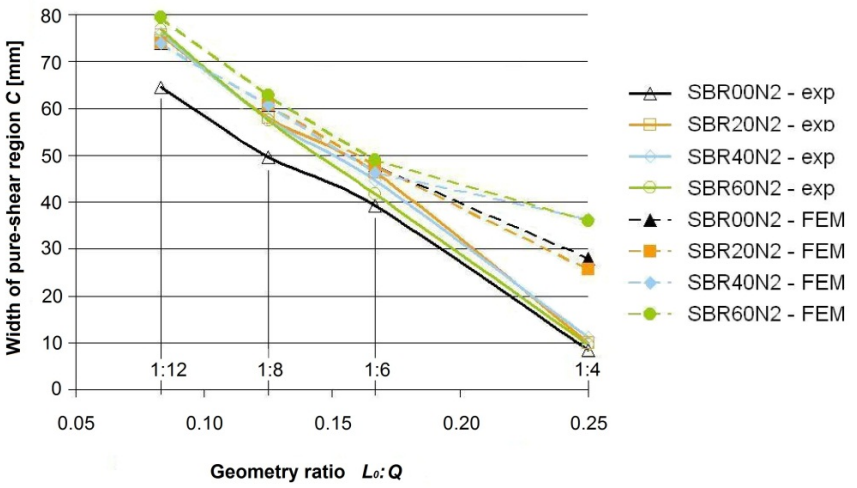

Fig. 19 Influence of the test specimen's geometry ratio on the width of pure-shear region *C,* evaluated experimentally as well as numerically at a maximum strain of 100% of the test specimen's length L_0

Figure 19 shows more detailed information about the coupling effect between the geometry ratio $L_0 : Q$ and the width of the pure-shear region C evaluated at a maximum strain of 100% of the test specimen's length L_0. A comparison of FEM results and experimental data is plotted in the diagram. By increasing the geometry ratio $L_0 : Q$ we determined a decrease in the width of the pure-shear region C. This effect was evaluated with FEM as well as with experimental methods. Clearly, both of the analysis methods show an accordant value of the pure-shear region's width C in the range of the geometry ratio from 1:12 to 1:6. The different values evaluated with FEM in comparison to the experimental method at the geometry ratio 1:4, are caused due to the optical method used for determination of the stretched white squared layer.

It is possible to correlate the observed dependence of the test specimen's geometry ratio on the width of pure-shear region C. We derived the following equation for C as a function of the strain in the range from 10 to 50% of the test specimen's length L_0:

$$C = \left[-3{,}115 \cdot \frac{L_0}{Q} + 0{,}979 - \kappa \cdot \varepsilon \right] \cdot 100\,, \tag{18}$$

where: $\kappa = 0{,}0905$ [-] - factor described the influence of strain,
ε [-] - strain.

Then, making use of this definition, we can propose the equation of minimal efficient notch length for the analysis of crack propagation in the pure-shear region:

$$a_{s0\min} = \frac{Q}{2} \cdot \left[1 - \frac{C}{100} \right]. \tag{19}$$

With the last equation, it is possible to perform a crack growth analysis in the pure-shear test specimen with a defined minimal notch length.

4.4 Dynamic Crack Growth Analysis by a New Method of Simultaneous SENT- and Pure-Shear-Mode Testing

Evaluation of Crack Growth Velocity Dependent on Test Specimen's Geometry Ratio L_0:Q and Notch Length

This experimental analysis has been performed by a new method of simultaneous SENT- and pure-shear-mode testing. Four SENT test specimens with single edge notches and three pure-shear test specimens with double edge notches were simultaneously analyzed in the Tear Analyzer. All the test specimens were based on the compound SBR20N2. Each of the SENT test specimens was notched with a notch length of a_0 = 2.0 mm. Two of the three pure-shear test specimens were notched with a notch length of a_0 = 21.0 mm and the last pure-shear test specimen was notched with a notch length of a_0 = 2.0 mm, identical to the SENT test specimens. The quantity of test specimens enables the tester to obtain and describe four crack growth curves according to all of the analyzed SENT and pure-shear test specimens with the notch length a_0 = 21.0 mm and two crack growth curves according to the last pure-shear test specimen with the notch length a_0 = 2.0 mm. The fatigue test conditions were set at a frequency of 1Hz, loading amplitude 25% of L_0, preload of test specimens 1N and the tests were performed in a laboratory atmosphere.

The averaged values of crack growth curves for each of the analyzed test specimens and relevant calculated crack growth velocities are shown in the Figure 20. The relationship between the crack growth length and number of cycles is visualized in diagram (I). The averaged value of crack growth in the SENT test specimen is the curve denoted (a). The curve can be divided into two different regions. In the first region the crack growth curve linearly increases as long as the crack length $a < 3.5$ mm and the increase is given at an angle of ξ_{T1}. In the second region, the crack propagates by a non-defined function of growth. A similar average of crack growth curves was observed in the pure-shear test specimen notched with the notch length a_0 = 2.0 mm, denoted (c). However, compared to the crack growth in SENT, three different regions of crack growth in the pure-shear test specimen were established. The linearity of crack growth curve occurs until a maximum crack length of $a < 3.0$ mm and is characterized by the angle $\xi_{T2} \approx \xi_{T1}$. The next region, indicated as non-defined crack growth function, has a curve

similar to the crack growth in the SENT test specimen. Because of the large width Q of the pure-shear test specimen, the crack growth proceeds in the last region of the second part of the linear increase of crack growth characterized by $\xi_{P2} > \xi_{T2}$. The second linearity of crack growth in the pure-shear test specimen (c) starts with a crack length $a < 22.0$ mm and continues over a broad range of crack lengths. The curve, denoted (b_1), represents the average value of crack growths in the pure-shear test specimens notched with the notch length $a_0 = 21$ mm. A linear relationship between crack length and number of cycles was observed in the complete range of analyzed cycles. The corresponding slope is ξ_{P1}. The horizontal translation of the curve (b_1) to the position (b_2) shows an increase similar to the second linear part of the crack growth curve (c), obtained in the pure-shear test specimen with the notch $a_0 = 2.0$ mm.

The following equation was used for the calculation of the crack growth velocities a' shown in the lower diagram (II) derived from the crack growth rate visualized in the upper diagram (I):

$$a'_{i+5} = \left(\frac{a_{i+5} - a_i}{t_{i+5} - t_i} \right); i \in <1, j>, \tag{20}$$

where t is a time dependent on cycles n, and j is the total number of measured values of crack lengths during the complete analysis. The calculations unambiguously show the constant crack growth velocity a' in the regions of crack growth linearity, and also proved the independence of the test specimen's geometry and notch length in this region. The non-defined crack growth curve in the range of crack length $3.0 \leq a \leq 22.0$ mm was characterized as a second derivation of crack length and thus represents an increasing acceleration of crack growth.

The experimental results suggest a common pattern of crack growth in rubber test specimens, demonstrate the complexity of the crack growth curve and describe the dependence of crack growth behavior on the test specimen's geometry ratio over the broad scale of the crack length.

The comparison of the crack growth curves obtained for different geometry ratios recognize the independence of the crack growth curve from the geometry ratio, whereas the variation of the ratio has been reached by the modification of a test specimen with width Q and invariable length L_0. The maximum possible crack length by the crack growth is then indirectly proportional to the geometry ratio. Thus, the description of a crack growth curve over a broad crack length scale can be obtained only in a test specimen with a low geometry ratio, as is demonstrated with the crack growth curve in the test specimen with the ratio $L_0 : Q = 1:8$.

Three regions characterized with different crack growth behavior have been identified in the crack growth curve as dependent on the crack length. The first narrow region of short crack length, where the crack propagates under a constant crack growth velocity, is characterized by a stable state of crack propagation.

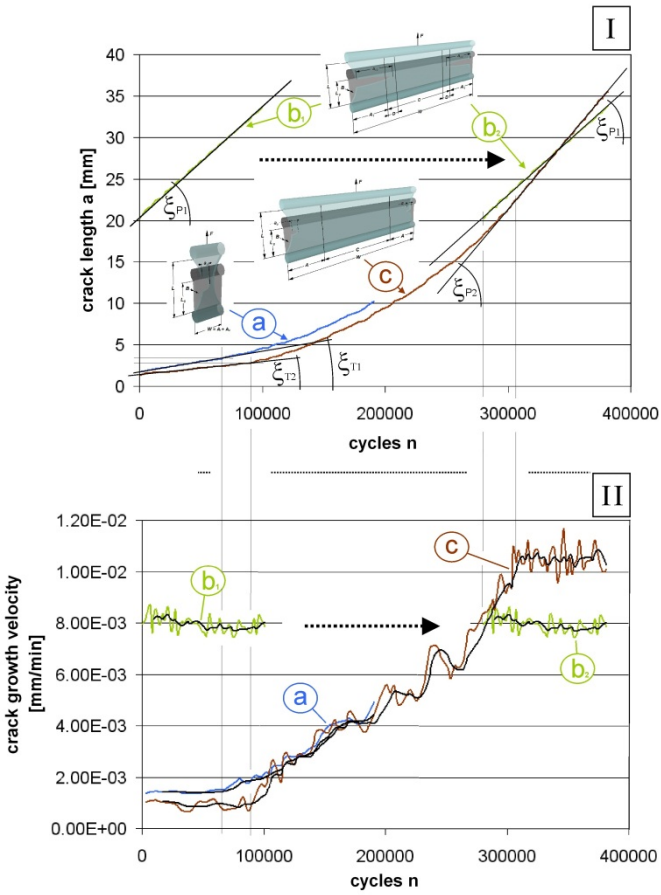

Fig. 20 Comparison of the crack growth rate (I) and calculated crack growth velocities (II) in the SENT and pure-shear test specimens for variable notch lengths

The crack growth curve occurs in this region independent from the geometry ratio. This approach was confirmed by FEM results (s. Figure 6), where the linear crack growth curve was confronted with tearing energy according to the expression in equation (9). The linear character of the crack growth allows for applying a very short notch length, which is a good premise to utilize the availability of the maximum length of the region of equation (9). However, on the other hand, the understanding of this approach guarantees the economic utilization of the test machine, represented by the termination of the analysis and leaving the stable state of crack propagation or availability of equation (9) for the analysis of the fracture mechanic in the SENT test specimen. This approach offers a hypothesis of the

common usage of double notch test specimens (DENT) with a high geometry ratio and thus improves the quantity of measured data.

In the second narrow region of the crack growth curve, an accelerated propagation of crack has been determined. According to the FEM simulation, this crack growth curve shows complicated progression and represents a transition to stable crack growth in the pure-shear region.

This very important pure-shear region is situated over a broad crack length scale in the center of test specimen. However, it is defined by the low geometry ratio and occurs in the complete center only in the single edge notched test specimen. In this region, the characteristics of dynamic crack growth are given by stable crack growth in pure-shear region characterized by the equation (13) and are consistent with FEM simulation. This approach defines the utilization of the pure-shear test specimen and proves there is also a presence of the pure-shear state in the test specimen with the higher geometry ratio. For extremely high values of the geometry ratio approaching 1, there is no more pure-shear region in the test specimen. As the result of the FEM shows for the double-notched test specimen with the low geometry ratio, there is a region near the center of test specimen, where the double-notched test specimen does not show the pure-shear state. This region is characterized by the two crack tips, where the distance between them decreases, and thereby the stress fields around the crack tips influence each other and the fracture behavior changes.

Experimental Fatigue Crack Growth Analysis

The tests were carried out through a new method of simultaneous tensile and pure-shear mode testing. The fracture mechanical investigations under cyclic loading were performed with four tensile and three pure-shear test specimens. Four tensile test specimens were represented with three notched SENT and one not-notched tensile test specimen with the identical geometry ratios: $L_0 : Q$ = 1:1. The three simultaneously analyzed pure-shear test specimens were represented with two notched and one non-notched test specimen with the identical geometry ratios: $L_0 : Q$ = 1:8. Measurements were performed with preloading force 1N under sinusoidal loading conditions with the frequency 1 Hz at room temperature. The strain was varied between 5% and 45 %. The list of analyzed compounds or detailed testing and boundary conditions of the experimental fatigue crack growth analysis are summarized in Table 4.

For the evaluation of tearing energy T_t in the SENT test specimen, the equation (9) was used, and of tearing energy T_p in the pure-shear test specimen, the equation (13) was used. For the evaluation of crack growth rate *da/dn,* dependent on tearing energy T_t *and* $T_{p,,}$ the automatic evaluation of strain energy density *w* of each loading cycle was used in combination with an optical detection of crack length *a* implemented in the Tear Analyzer. The determined data were summarized to the double logarithmic plot of crack growth rate vs. tearing energy. This type of power law behavior is termed “Paris Plot” and expressed with the equation (16).

Table 4 Testing and boundary conditions for the fatigue crack growth analysis

Compound			Loading mode		Sinusoidal	
No.	Label		No. of frequencies		1	[Hz]
1.	NR00N2		List of loading amplitudes		5; 10; 13; 16; 20; 25; 30; 35; 40; 45	[%]
2.	NR20N2					
3.	NR40N2					
4.	NR60N2		Test specimen geometry (L_0 x Q x B)			No. of test specimens analyzed per amplitude
5.	SBR20N2					
6.	SBR40N2		Tensile	15x15x1,5	[mm]	4
7.	SBR60N2		Pure-shear	15x120x1,5	[mm]	3
8.	EPDM20N					
9.	EPDM40N		Notch length a_0			Type of notch
10.	EPDM60N		Tensile	2	[mm]	SEN (single edge notch)
11.	S-NR60N2		Pure-shear	21	[mm]	DEN (double edge
12.	S-E60N2N					
13.	S-E60N2M		Type of crack growth observation			Outline

In Figure 21, the influence of the volume of carbon black in NR on crack growth rate becomes apparent. We found that the crack growth rate at a given tearing energy decreases significantly with an increase in the volume of carbon black, whereas the crack growth exponent m slightly increases with a higher amount of carbon black in rubber test specimens based on NR. The increase of tear strength independent from carbon black concentration induces the higher crack growth rate. However, at the integration of an increasing concentration of carbon black, the tear resistance becomes higher. This indicates the positive reinforcement of NR by carbon black type N234. The increase of the crack growth exponent m pointed to the decreasing influence of the reinforcement with carbon black at higher tearing energies.

The simultaneous analyzation of two different test specimens determined the dependence of crack growth rate on tearing energy, by detecting the identical crack growth exponent m in the both of the test specimens. The comparison of the results determined in SENT as well as in pure-shear test specimens visualized in Figure 21, shows that the crack growth rate at a given tearing energy is higher in the pure-shear in comparison to the SENT test specimen, as observed in the non-reinforced and reinforced NR with a concentration of 20 phr of carbon black. The trends of the crack growth rate at the given tearing energy of NR reinforced by the concentration of 40 phr of carbon black are identical, as evaluated in SENT as well as in pure-shear test specimens.

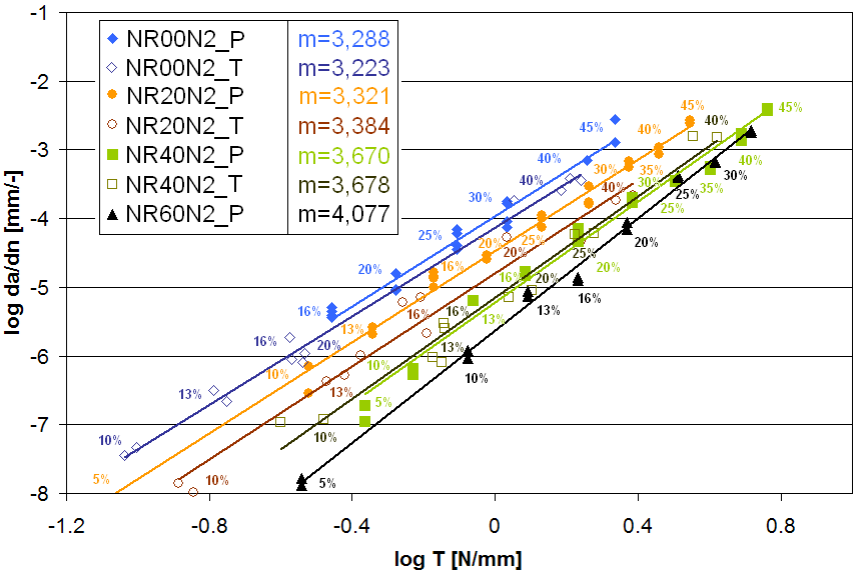

Fig. 21 Power law behavior of fatigue crack growth rate vs. tearing energy for the SENT (denoted T) as well as pure-shear (denoted P) test specimens based on carbon black filled NR

Figure 22 shows the effect of filler concentration in SBR on fatigue crack growth rates. Similar trends as in NR of dependence of fatigue crack growth rate on tearing energy are observed in SBR. With an increase of carbon black concentration, the decrease of the crack growth rate at a given tearing energy has been determined. It was found that the crack growth exponent *m* slightly decreases with a higher concentration of carbon black in rubber test specimens based on SBR.

The comparison of the results determined in SENT as well as in pure-shear test specimens proved a higher crack growth rate at a given tearing energy in the pure-shear as compared to the SENT test specimens. These trends have been observed in the all of the reinforced SBR test specimens independent from carbon black concentration. The result showed the identical crack growth exponent *m* independent from the test specimen's geometry.

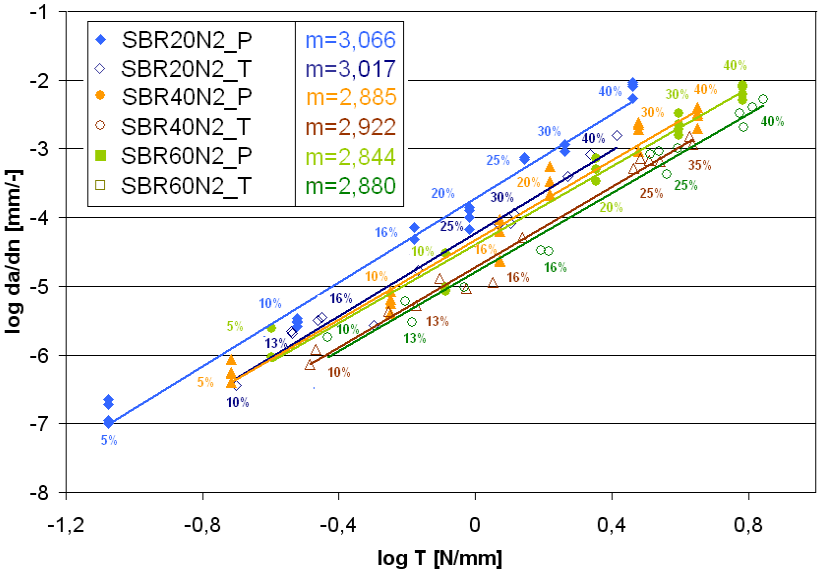

Fig. 22 Power law behavior of fatigue crack growth rate vs. tearing energy for the SENT (denoted T) as well as pure-shear (denoted P) test specimen based on carbon black filled SBR

Obviously, the crack growth exponent *m* observed in the reinforced EPDM (s. Figure 23) is significantly lower in comparison to the crack growth exponents determined in the reinforced NR and SBR. The crack growth exponent characterized by the dynamic fracture behavior of EPDM is not dependent on carbon black concentration. The increase of carbon black concentration has a decreasing influence on crack growth rate at a given tearing energy in SENT as well as in pure-shear test specimens based on EPDM. The comparison of the influence of a test specimen's geometry on dynamic fracture behavior in EPDM showed that the crack growth rate at a given tearing energy in the pure-shear test specimen is higher compared to the crack growth rate in the SENT test specimen.

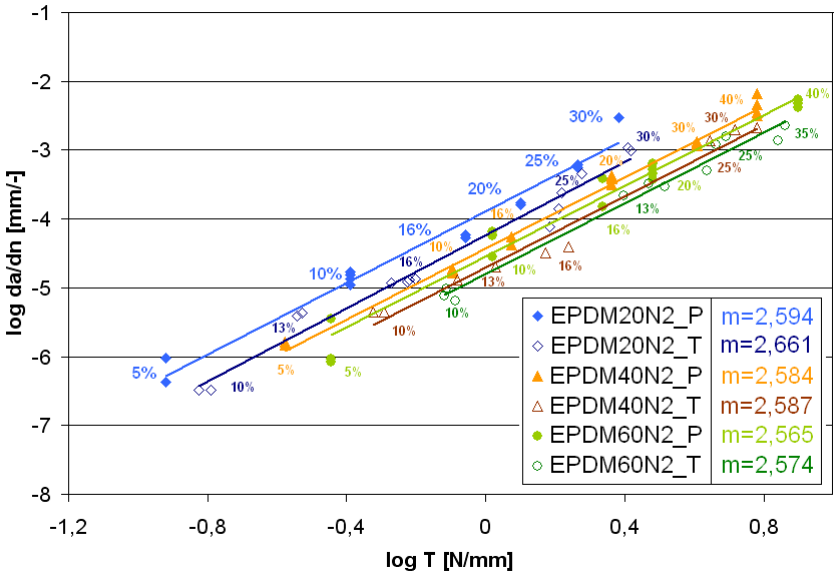

Fig. 23 Power law behavior of fatigue crack growth rate vs. tearing energy for the SENT (denoted T) as well as pure-shear (denoted P) test specimen based on carbon black filled EPDM

It was assumed that the behavior of the fatigue crack growth rate vs. the tearing energy of a blend based on two different rubbers depends on the fracture behavior of each type of rubber used. In Figure 24, we analyzed and plotted a comparison of power law behavior of fatigue crack growth rate vs. tearing energy for SBR, NR and blend SBR-NR based polymers, reinforced with 60 phr of carbon black type N234. We found that the crack growth rate at a given tearing energy of blend S-NR60N2 (based on 50phr of SBR and 50phr of NR) is derived from the fracture behavior of the individual components SBR and NR, because of the localization of the fracture values of blends between the fracture values of the both components. The crack growth rate at a given tearing energy of blend S-NR60N2 is closer to the fracture behavior of the NR component in comparison to the fracture data of the SBR component. This phenomenon shows the dominant influence of NR on the crack propagation in a blend based on SBR and NR.

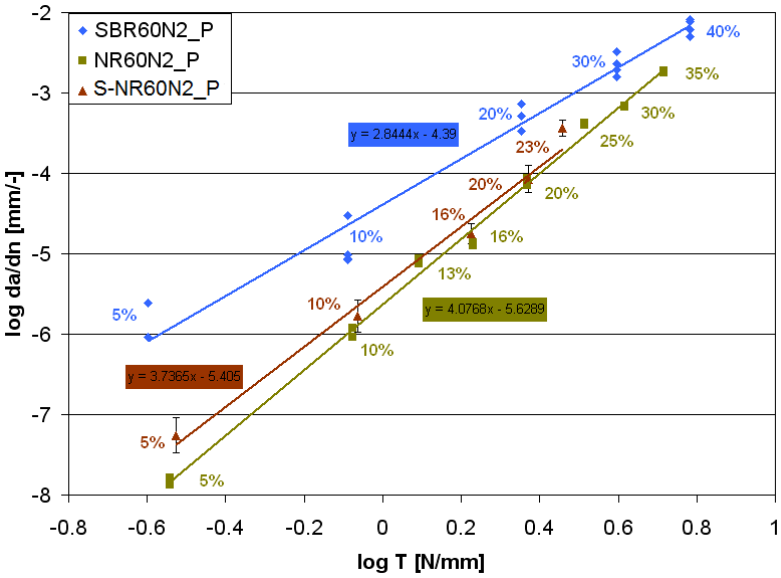

Fig. 24 Comparison of power law behavior of fatigue crack growth rate vs. tearing energy for SBR, NR and blend SBR-NR based polymers reinforced with 60 phr of carbon black type N234

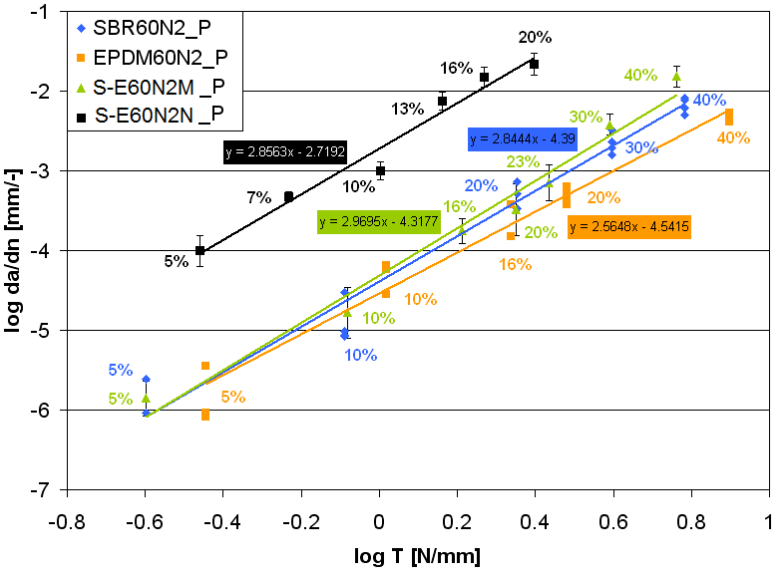

Fig. 25 Comparison of power law behavior of fatigue crack growth rate vs. tearing energy for SBR, EPDM and blend SBR-EPDM based polymers reinforced with 60 phr of carbon black type N234 normal or N234 master batch

In addition to this observation, the blend S-E60N2N, based on SBR and EPDM with 60phr of carbon black type N234 normal and the blend S-E60N2M, based on SBR and EPDM with 60phr of carbon black type N234 master batch were analysed dynamically in the Tear Analyser. The related results of these experiments are shown in Figure 25. The data of the crack growth rate at a given tearing energy for blend S-E60N2M are similar with the fracture behavior determined in the component SBR. Thus the component SBR is the main factor influencing the fracture mechanic of blends. The blend S-E60N2N has a lower dynamic crack growth resistance compared to the fracture behaviour of SBR, EPDM as well as blend S-E60N2M. The higher dynamic crack growth resistance of S-E60N2M could be reached by the increasing activity of master batch carbon black that leads to an increasing number of polymer-filler interactions and therefore to a higher level of fracture mechanical properties.

5 Conclusion

The aim of this research work was to develop a new method for the description of dynamic crack growth behavior of rubber by simultaneous tensile and pure shear mode testing, and to systematize efficiently the analysis of fracture behavior of elastomers. For a study of fracture material behavior, industrially used test methods were selected carefully. The material investigated were SBR, EPDM, NR, blends SBR-NR and SBR-NR vulcanizates reinforced with different filler content. The results of the analysis show different information regarding the various fracture mechanisms and methods for the efficient description of fracture behavior of rubber.

At first, the work deals with the theoretical description of the dependence of fracture behavior in rubber test specimens on its geometry, respective in its geometry factors L_0:Q. We assumed numerically that the deformation in the pure-shear test specimen is close to the pure-shear state in the center. However, the deformation in the regions near the free edges is complex. We demonstrated similar crack growth behavior in the free edges of SENT as well as of pure-shear test specimens.

The development of a new method for the analysis of dynamic crack propagation in filled rubbers by simultaneous tensile and pure shear mode testing is shown. The development is based upon the mechanical redevelopment of the test machine 'Tear Analyzer' (Co. Coesfeld GmbH), upon the equipment of the test machine with new hardware, and modification of the system for the recording of crack length. This machine is equipped with two modes operating simultaneously, which represents an extended fracture testing method. The redevelopment of the machine for the measurement of pure-shear test specimens was conditioned with the determination of test measurement accuracy. The FEM method was used for the calculation of the dynamic behavior of the machine's design in the range of used frequencies. The FEM calculation showed the weak

points of the design and pointed out the necessary steps of redevelopment for measurement in the range of frequencies from 0.1 to 20 Hz.

The next objective was to investigate and to define the minimum length of a notch for the initiation of crack propagation in a pure-shear test specimen for the analysis of dynamic crack propagation in rubber. Test specimens with different geometry factors L_0:Q in the range of 1:12 to 1:4, with or without initial cracks have been investigated. The newly developed experimental method was supplemented by an appropriate FE–analysis. These methods firstly allowed a determination of the width of the pure-shear range, and thus a definition of the minimal notch length in the test specimen independent from its geometry. This definition forms the theoretical basis for an improvement in the efficiency of the analysis of dynamic crack propagation in rubbers.

The definition of the notch length had to be supported with the development of a method for the defined insertion of a notch into a rubber specimen. This method serves as a basis for the reproducible and reliable determination of fracture mechanical parameters for elastomers. After insertion of notches in a defined way, fracture tests under quasi-static loading conditions were performed. A significant influence on the notch geometry was observed in the test results. The variation of the angles of the notch showed a strong influence on the crack propagation. These results illustrated the importance of a defined and reproducible notching of elastomeric specimens.

In the experimental study of dynamic fracture behavior, experimental crack growth data of several rubber test specimens were obtained simultaneously with a new mechanical fracture testing concept. The test specimen used had different geometry ratios from those represented by commonly used SENT and pure-shear test specimens. This testing concept allowed a direct comparison of the dynamic crack growth behavior dependent on the test specimen's geometry ratios. We demonstrated the application of this testing method for the description of fracture behavior dependent on arbitrary crack lengths. The comparison of experimental data and FEM results show a dependence of the tearing energy on the crack growth curve and, thus, the correspondence between the regions of stable crack growth propagation obtained in experimental tests and regions of calculated tearing energy. The results identified the weak points of the dynamic crack growth analysis in such rubber test specimens and suggests steps for a follow-up research.

We found from the dynamic fracture investigation that the crack growth rate at a given tearing energy decreases significantly with increasing carbon black content, independent from the base of rubber. The results demonstrated the increase of the crack growth exponent m according to the strain. The decreasing influence of reinforcement with carbon black at higher tearing energies is shown. The dependence of crack growth rate vs. tearing energy simultaneously analysed in two different test specimens detected the identical crack growth exponent m in both of the test specimens. The comparison of the results determined in SENT as well as in pure-shear test specimens shows that the crack growth rate at a given tearing energy is higher in the pure-shear compared to the SENT test specimen, independent from the base of rubber. Therefore, the pure-shear test specimen

represents a more critical geometry for the determination of fracture behavior of rubber.

The concept of simultaneously testing of SENT and pure-shear test specimens represents a new method for the improved description of the dynamic fracture behavior of rubber materials.

References

[1] Rivlin, R.S., Thomas, A.G.: Rupture of rubber. I. Characteristic energy for tearing. Journal of Polymer Science 10, 291–318 (1953)
[2] Lake, G.J., Lindley, P.B.: Cut Growth and Fatigue of Rubbers, II. Experiments on a Noncrystallizing Rubber. Journal of Applied Polymer Science 8, 707–721 (1964)
[3] Lake, G.J., Lindley, P.B.: The Mechanical Fatigue Limit for Rubber. Journal of Applied Polymer Science 9, 1233–1251 (1965)
[4] Stoček, R., Heinrich, G., Gehde, M., Rauschenbach, A.: Untersuchungen zur Kerbtiefe im Pure-shear Prüfkörper für präzise Analysen der dynamischen Rissausbreitung in Elastomeren. Zeitschrift Kunststofftechnik / Journal of Plastics Technology, 2–22 (January 2012)
[5] Yeoh, O.H.: Analysis of deformation and fracture of 'pure shear' rubber testpiece. Plastics, Rubber and Composites 30, 391–397 (2001)
[6] Griffith, A.A.: The phenomena of rupture and flow in solids. Philos. Trans. R. Soc. Lond., Ser. A 221, 163 (1920)
[7] Lake, G.J.: Fatigue and Fracture of Elastomers. Rubber Chemistry and Technology 68, 435–460 (1995)
[8] Klüppel, M., Huang, G., Bandow, B.: Evaluation of Tearing Energy of Elastomer Materials. Kautschuk-Gummi-Kunststoffe 61, 656–659 (2008)
[9] Gent, A.N.: Engineering with Rubber, 2nd edn. Hanser Publishers, Munich (2001)
[10] Gent, A.N., Lindley, P.B., Thomas, A.G.: Cut Growth and Fatigue of Rubbers. I. The Relationship between Cut Growth and Fatigue. Journal of Applied Polymer Science, 455–466 (1964)
[11] Paris, P., Erdogan, F.: A critical analysis of crack propagation laws. Journal of Basic Engineering, Transactions of the American Society of Mechanical Engineers, 528–534 (1963)
[12] Stoček, R., Gehde, M., Heinrich, G.: Analyse des dynamischen Risswachstums von Elastomeren im simultanen Zug-(Tensile-) und Pure-Shear-Prüfmodus bei optimierter Risserfassung. Kautschuk-Gummi-Kunststoffe 62, 170–176 (2009)